



Scienxt Journal of Physics and Space Science  
Volume-2 || Issue-1 || Jan-June || Year-2024 || pp. 1-9

## *Aurvillius oxide introduction, materials characterization: literature review*

**\*<sup>1</sup>Shivangi Dubey, <sup>2</sup>Azam Ansari, <sup>3</sup>Shahnawaz Ansari, <sup>4</sup>Rahul Gupta**

<sup>\*1</sup>Assitant Professor, Department of Basic Science, Bhopal Institute of Technology and Science, Bhojpur Road Bhopal,  
462045 M.P. India

<sup>2,3,4</sup>Student, Department of Basic Science, Bhopal Institute of Technology and Science, Bhojpur Road Bhopal, 462045 M.P.  
India

*\*Corresponding Author: Shivangi Dubey  
Email: shivangidubeymanit@gmail.com*

## **Abstract:**

The synthesis of Aurivillius phase layered bismuth titanate ( $\text{Bi}_4\text{Ti}_3\text{O}_{12}$ , BTO) thin films on FTO glass substrates via sol-gel spin coating technique and their potential for detecting mercury ( $\text{Hg}^{2+}$ ) and lead ( $\text{Pb}^{2+}$ ) ions are investigated. XRD analysis indicates predominant crystal growth along the (117) plane, indicative of the orthorhombic structure of BTO. SEM images reveal an anisotropic plate-like morphology. Photoluminescence The thickness of the deposited film is influenced by the viscosity of the coating solution and the rotational speed during the spin-coating process. By adjusting cence spectra exhibit a prominent optical emission peak at 545 nm, with observed phonon modes consistent with the orthorhombic phase of BTO thin films. Electrochemical studies demonstrate the high electrochemical activity of the fabricated thin film electrode in detecting mercury ( $\text{Hg}^{2+}$ ) and lead ( $\text{Pb}^{2+}$ ) ions, boasting enhanced sensitivity and low detection limits.

## 1. Introduction:

Bismuth titanate ( $\text{Bi}_4\text{Ti}_3\text{O}_{12}$ ) stands out as a bismuth-based layered ferroelectric oxide within the Aurivillius layer-type compound family. Renowned for its Perovskite structure, this material exhibits distinct orthorhombic characteristics, leading to plate-like crystal growth. The compound's structure can be represented by the general formula  $\text{Bi}_2\text{O}_2(\text{Mn}_{1-1}\text{RnO}_{3n+1})_2$ , comprised of alternating layers of  $\text{Bi}_2\text{O}_2$  and  $\text{Mn}_{1-1}\text{RnO}_{3n+1}$  Perovskite layers (Villegas et al., 1996). Fig. 2.1. Illustrates the arrangement of layers in bismuth titanate.

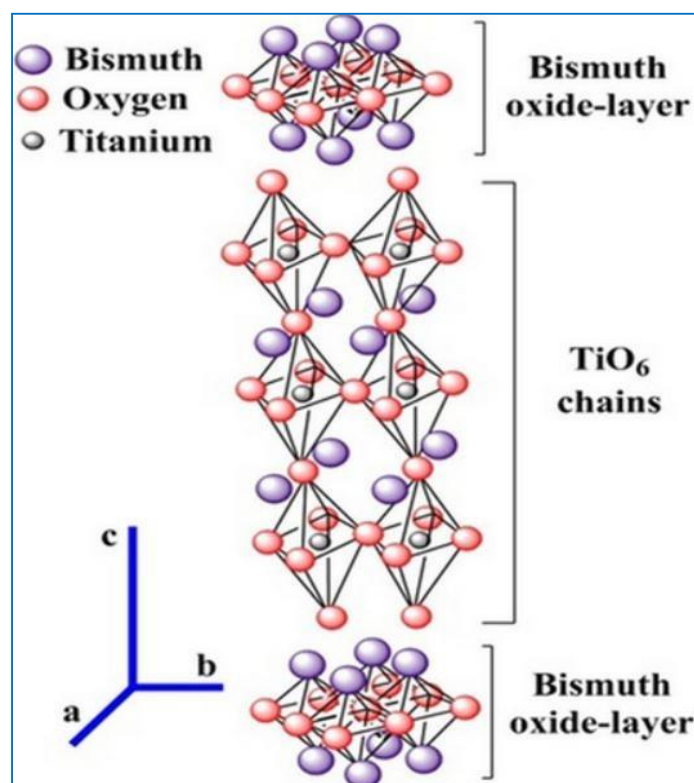


Figure. 2.1: Schematic illustration of  $\text{Bi}_4\text{Ti}_3\text{O}_{12}$  (Ambriz-Vargas et al., 2017)

In the general formula, the value of  $n$  ranges between 1 and 7. The formula unit  $(\text{Mn}_{1-1}\text{RnO}_{3n+1})_2$  comprises pseudo perovskite units interleaved between layers of  $(\text{Bi}_2\text{O}_2)_2$ . Here,  $M$  represents a large monovalent ( $\text{Na}^+$ ), divalent ( $\text{Pb}^{2+}$ ), or trivalent cation ( $\text{Bi}^{3+}$ ), typically an alkali or alkaline earth cation, while  $R$  denotes a diamagnetic transition metal, which can be trivalent ( $\text{Fe}^{3+}$ ), tetravalent ( $\text{Ti}^{4+}$ ), pentavalent ( $\text{Ta}^{5+}$ ), or hexavalent ( $\text{W}^{6+}$ ) (Umabala et al., 2000).

The  $\text{Bi}_4\text{Ti}_3\text{O}_{12}$  phase exhibits a Curie temperature of  $675^\circ\text{C}$ , characterized by high dielectric power and a dielectric constant of approximately 200. At room temperature,  $\text{Bi}_4\text{Ti}_3\text{O}_{12}$  adopts a monoclinic structure. Below  $600^\circ\text{C}$ , it transitions to a tetragonal phase, while above  $750^\circ\text{C}$ , it undergoes a transformation from tetragonal to orthorhombic. Its electrical conductivity

displays strong anisotropy, with the highest conductivity occurring within the plane of polarization. Remarkably, the optical indicator exhibits peculiar rotation upon polarization switching.

Within the ternary Bi-Ti-O system, numerous other bismuth titanates exist alongside the ferroelectric Bi<sub>4</sub>Ti<sub>3</sub>O<sub>12</sub>, including Bi<sub>2</sub>Ti<sub>2</sub>O<sub>7</sub> and Bi<sub>12</sub>Ti<sub>10</sub>O<sub>20</sub>. Additionally, Speranskaya et al. (1965) documented two more bismuth titanate phases, Bi<sub>8</sub>Ti<sub>10</sub>O<sub>14</sub> and Bi<sub>2</sub>Ti<sub>4</sub>O<sub>11</sub>.

## 2. Properties of bismuth titanate (Bi<sub>4</sub>Ti<sub>3</sub>O<sub>12</sub>):

Bismuth titanate exhibits the following properties:

- High remnant polarization
- Low coercive field
- Superior fatigue resistance
- High Curie temperature
- Low processing temperatures
- Large electro-optical coefficient
- Low leakage current
- Low dielectric loss and high electrical resistivity
- High dielectric and piezoelectric constants (Xu et al., 2003)

### 2.1. Applications of bismuth titanate (Bi<sub>4</sub>Ti<sub>3</sub>O<sub>12</sub>):

Thin films of bismuth titanate have been extensively investigated for various applications, including:

- Photoelectric switching behavior applications
- Nonvolatile ferroelectric random access memories (FeRAMs)
- High-temperature piezoelectric applications
- Multifunctional devices utilized in microelectronics and optoelectronics (Sedlar and Sayer, 1996)
- Spin Coating Theory
- The spin-coating technique is employed to fabricate uniform thin films ranging from

micrometers to nanometers in thickness. This method involves placing the substrate on a chuck that rotates the sample, causing the liquid to spread radially outward. The primary mechanisms responsible for achieving flat deposition on the surface include viscous forces and surface stress. Subsequently, evaporation occurs, resulting in the formation of the thin film.

- Spin Coating Method
- Spin coating is a process for producing thin, uniform organic films over large areas, typically with diameters up to 30 cm. The procedure involves four main steps: fluid dispense, spin up, stable fluid outflow, and spin-off followed by evaporation, as illustrated in Figure 2.2.
- Initially, the material is deposited onto the turntable, then spun up and spun off sequentially, with evaporation occurring concurrently. Centrifugal force disperses the applied solution across the turntable, causing the layer to thin as the spinning speed increases. Subsequently, the obtained layer undergoes drying. The rapid rotation facilitates uniform evaporation of the solvent, with high-volatile components being removed from the layer, while low-volatile components remain on the surface (Nguyen et al., 2012).

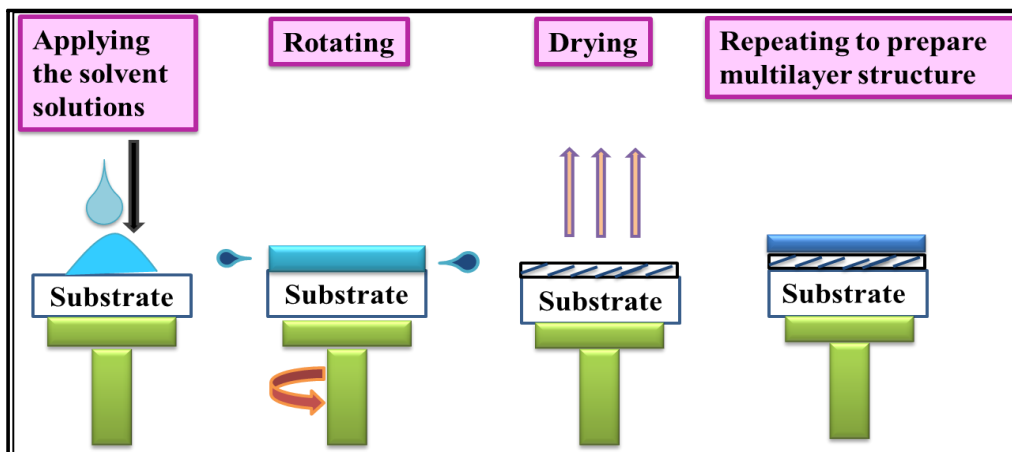


Figure. 2.2: Different steps for spin coating technique

### 3. Stages of the spin coating method:

The spin coating process consists of four stages: deposition, spin-up, spin-off, and evaporation, as depicted in Fig. 2.3. Initially, the material is deposited onto the turntable, followed by sequential spin-up and spin-off steps, during which evaporation occurs concurrently. Centrifugal force evenly distributes the applied solution across the turntable, resulting in thinning of the layer as the spinning speed increases. The rapid rotation facilitates

uniform evaporation of the solvent. During evaporation, high-volatile components of the solution are removed from the layer, while low-volatile components remain on the surface (Sahu et al., 2019). The thickness of the deposited film is controlled by the viscosity of the coating solution and the rotational speed.

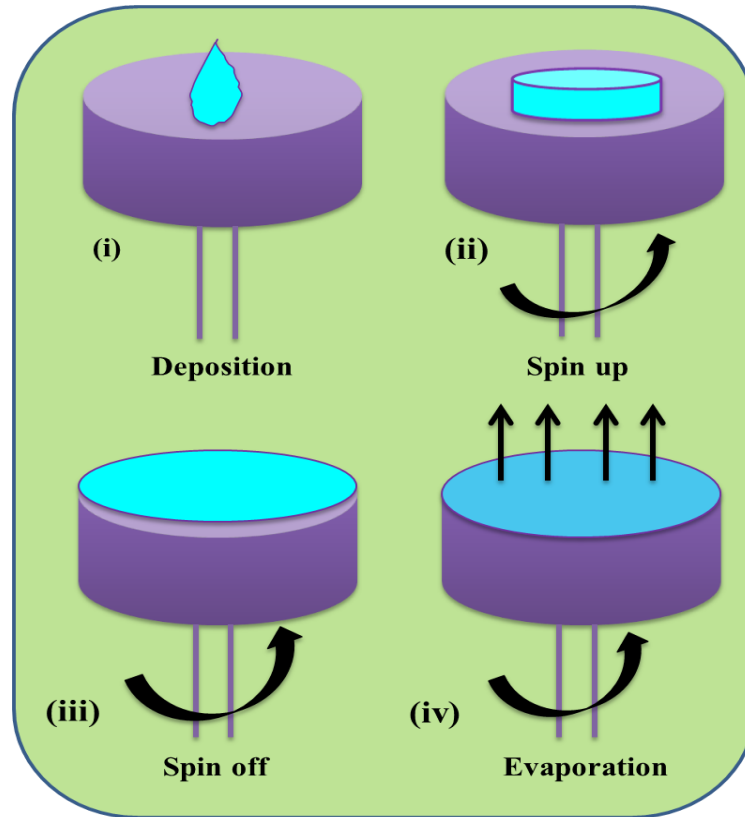


Figure. 2.3: Different stages of the spin coating method

### 3.1. The thickness of the film:

The thickness of the deposited film is influenced by the viscosity of the coating solution and the rotational speed during the spin-coating process. By adjusting these parameters, the desired film thickness can be achieved. Several factors contribute to determining the film thickness, as illustrated in the equation below

$$h = \left(1 - \frac{\rho_A}{\rho_{A0}}\right) \cdot \left(\frac{3\eta \cdot m}{2\rho_{A0} \omega^2}\right)^{1/3}$$

Where  $h$  is thickness,  $\rho_A$  is volatile liquid density,  $\eta$  is solution viscosity,  $m$  is evaporation rate, and  $\omega^2$  is angular speed since the evaporation rate is determined experimentally, the following equation has been proposed:

$$h = A\omega - B$$

$B$  is a constant parameter that was measured experimentally. In the vast majority of cases,  $B$

is between 0.4 and 0.7. It follows from this equation that the higher the angular speed of the substrate, the thinner the film will be (*Makhlouf et al., 2011*).

#### **4. Advantages and disadvantages of the spin coating method:**

##### **4.1. Advantages:**

Compared to vapor-phase deposition methods, there is minimal material loss.

It is a cost-effective technique; a rotating plate is significantly less expensive than a vacuum deposition apparatus.

- Thin layers can be deposited quickly and easily using spin coating.

##### **4.2. Disadvantages:**

- Creating multilayer structures with more than two layers is challenging.
- Contaminants such as traces of solvent, oxygen, and humidity may be present.
- Achieving precise control over deposition parameters like homogeneity and rugosity can be difficult.
- Producing highly thin films (less than 10nm) is impractical (*Boudrioua et al., 2017*)

#### **5. Materials characterization:**

To characterize the deposited thin films, a series of analytical techniques were employed. X-ray diffraction (XRD) analysis was conducted using an X'pert PRO PAN analytical instrument operating at 40 kV and 30 mA with CuK $\alpha$  radiation ( $\lambda=1.5418 \text{ \AA}$ ) to examine the crystal structure and crystallinity. Thickness measurements were performed using a Stylus Profilometer (Mitutoyo, S-301). The morphology of the films was investigated using a ZEISS Scanning Electron Microscope operated at 30 kV.

The oxidation state of the film was determined via X-ray Photoelectron Spectroscopy (PHI versa probe III). The crystal quality and presence of defects in the deposited films the thickness of the deposited film is influenced by the viscosity of the coating solution and the rotational speed during the spin-coating process. By adjusting were studied using Varian Eclipse optical emission properties. Photoluminescence spectroscopy was employed to evaluate the optical

emission properties of the films, utilizing a Varian Cary Eclipse Spectrophotometer under an excitation wavelength of 350 nm.

Optical absorbance and transmittance spectra were recorded using a UV-Vis-NIR spectrophotometer (Ocean Optics HR 2000). Additionally, cyclic voltammetric performance and Electrochemical Impedance Spectroscopy (EIS) were carried out using a CHI 760E over varying frequencies ranging from 10 Hz to 1 MHz. In the conventional three-electrode system utilized, the prepared thin film served as the working electrode, while platinum and Ag/AgCl were employed as the counter and reference electrodes, respectively.

## 6. Conclusion:

The report provides a comprehensive overview of the deposition process for both pure and doped bismuth titanate thin films using the sol-gel spin coating technique, along with their potential application in heavy metal sensing.

## 7. References:

- (1) Linden D D, Reddy TB. Handbook of batteries. Third Ed. The McGraw-Hill Companies, Inc; 2002.
- (2) Simon P, Yu Gogotski. Nat Mater 2008; 7:845e54. [https://doi: 10.1038/nmat2297](https://doi.org/10.1038/nmat2297).
- (3) Rabe K, Ahn CH, Triscone J. Physics of ferroelectrics: a modern perspective. Heidelberg: Springer; 2007.
- (4) Lines ME, Glass AM. Principles and applications of ferroelectrics and related materials. Oxford: Classic Text in the Physical Sciences; 2001.
- (5) Yang L, Kong X, Li F, Hao H, Cheng Z, Liu H, Li J, Zhang S. Prog Mater Sci 2019;102:72e108.
- (6) Lysne PC, Percival CM. J Appl Phys 1975; 46(4):1519e25. <https://doi.org/10.1063/1.321803>.
- (7) Setchell RE. J Appl Phys 2005; 97:013507.
- (8) Shkuratov SI, Baird J, Antipov VG, Talantsev EF, Jo HR, Valadez JC, Lynch CS. Appl Phys Lett 2014;104:212901.
- (9) Peng P, Nie H, Wang G, Liu Z, Cao F, Dong X. Appl Phys Lett 2018;113:082901.



- (10) Gao Z, Peng W, Chen B, Redfern SAT, Wang K, Chu B, He Q, Sun Y, Chen X, Nie H, Deng W, Zhang L, He H, Wang G, Dong X. Phys Rev Mater 2019;3. 035401, <https://DOI:10.1126/sciadv.aba0367>.
- (11) Liu Z, Lu T, Xue F, Nie H, Withers R, Studer A, Kremer F, Narayanan N, Dong X, Yu D, Chen L, Liu Y, Wang G. Sci Adv 2020;6(21):eaba0367. <https://doi.org/10.1002/adma.201701824>.
- (12) Altgilbers LL, Baird J, Freeman B, Lynch CS, Shkuratov SI. Explosive pulsed power. London: Imperial College Press; 2010.
- (13) Shkuratov SI. Explosive ferroelectric generators: from physical principles to engineering. World Scientific Publishing Co.; 2019. <https://doi.org/10.1142/10958>.
- (14) Shkuratov SI, Baird J, Antipov VG, Chase JB, Hackenberger WS. Appl Phys Lett 2019; 114:172902.
- (15) Shkuratov SI, Baird J, Antipov VG, Zhang S, Chase JB. Adv Mater 2019; 31: 1904819. <https://doi.org/10.1002/adma.201904819>.